Gating pore currents are defects in common with two Na$_v$1.5 mutations in patients with mixed arrhythmias and dilated cardiomyopathy

Adrien Moreau,[1] Pascal Gosselin-Badaroudine,[1] Lucie Delemotte,[2] Michael L. Klein,[2] and Mohamed Chahine[1,3]

[1]Centre de Recherche de L'Institut Universitaire en Santé Mentale de Québec, Québec City, Québec G1J 2G3, Canada
[2]Institute of Computational Molecular Science, Temple University, Philadelphia, PA 19122
[3]Department of Medicine, Université Laval, Québec City, Québec G1K 7P4, Canada

The gating pore current, also called omega current, consists of a cation leak through the typically nonconductive voltage-sensor domain (VSD) of voltage-gated ion channels. Although the study of gating pore currents has refined our knowledge of the structure and the function of voltage-gated ion channels, their implication in cardiac disorders has not been established. Two Na$_v$1.5 mutations (R222Q and R225W) located in the VSD are associated with atypical clinical phenotypes involving complex arrhythmias and dilated cardiomyopathy. Using the patch-clamp technique, in silico mutagenesis, and molecular dynamic simulations, we tested the hypothesis that these two mutations may generate gating pore currents, potentially accounting for their clinical phenotypes. Our findings suggest that the gating pore current generated by the R222Q and R225W mutations could constitute the underlying pathological mechanism that links Na$_v$1.5 VSD mutations with human cardiac arrhythmias and dilatation of cardiac chambers.

INTRODUCTION

Voltage-gated Na$^+$ (Na$_v$) channels are transmembrane proteins that are responsible for action potential (AP) initiation in several excitable cells. The *SCN5A* gene encodes Na$_v$1.5, the main Na$_v$ isoform expressed in the heart. This large 2,016–amino acid protein plays a pivotal role in the excitation–contraction process. Na$_v$1.5 mediates the rapid Na$^+$ upstroke, leading to cell depolarization and contraction. It is composed of 24 transmembrane segments organized in four homologous domains (DI–DIV) (Fig. 1). The first four transmembrane segments of each domain (S1–S4) form the voltage-sensor domain (VSD), and the assembly of the transmembrane segments S5 and S6 of the four homologous domains forms the pore domain. Usually, dysfunctions of Na$_v$1.5 channels cause well-described cardiac arrhythmias such as type 3 long QT syndrome, Brugada syndrome, or progressive cardiac conduction defect and sick sinus syndrome (Amin et al., 2010).

The Na$_v$1.5 R222Q and R225W mutations have recently been reported to be associated with the development of an atypical phenotype combining several cardiac arrhythmias and dilatation of cardiac chambers (Bezzina et al., 2003; Cheng et al., 2010; McNair et al., 2011; Laurent et al., 2012; Mann et al., 2012; Nair et al., 2012). These highly conserved R222 and R225 residues are located on the S4 segment of DI of the channel protein (Fig. 1). Although their clinical phenotypes share major similarities, highly divergent biophysical properties have also been observed (Table S1) (Bezzina et al., 2003; Cheng et al., 2010; Laurent et al., 2012; Mann et al., 2012; Nair et al., 2012). Indeed, the R222Q mutant channel exhibits gain of function characteristics, whereas the markedly lower current density observed for the R225W mutant channel leads to loss of function. Thus, so far, no common mechanism explains the similar phenotypes of R222Q and R225W mutations.

Using electrophysiology and molecular dynamics techniques, we investigated the biophysical properties of the R222Q and R225W mutant channels in search of a potentially unifying molecular mechanism that would explain the previously reported phenotypic manifestations. We discovered that the two mutations induce a cationic leak under depolarized condition. Furthermore, after long depolarization periods, we recorded gating pore currents under hyperpolarized conditions, probably caused by a freezing of the VSD after depolarization. As this leak through the VSD is the only alteration of the channel's properties common to both mutations, we

The Rockefeller University Press $30.00
J. Gen. Physiol. Vol. 145 No. 2 93–106
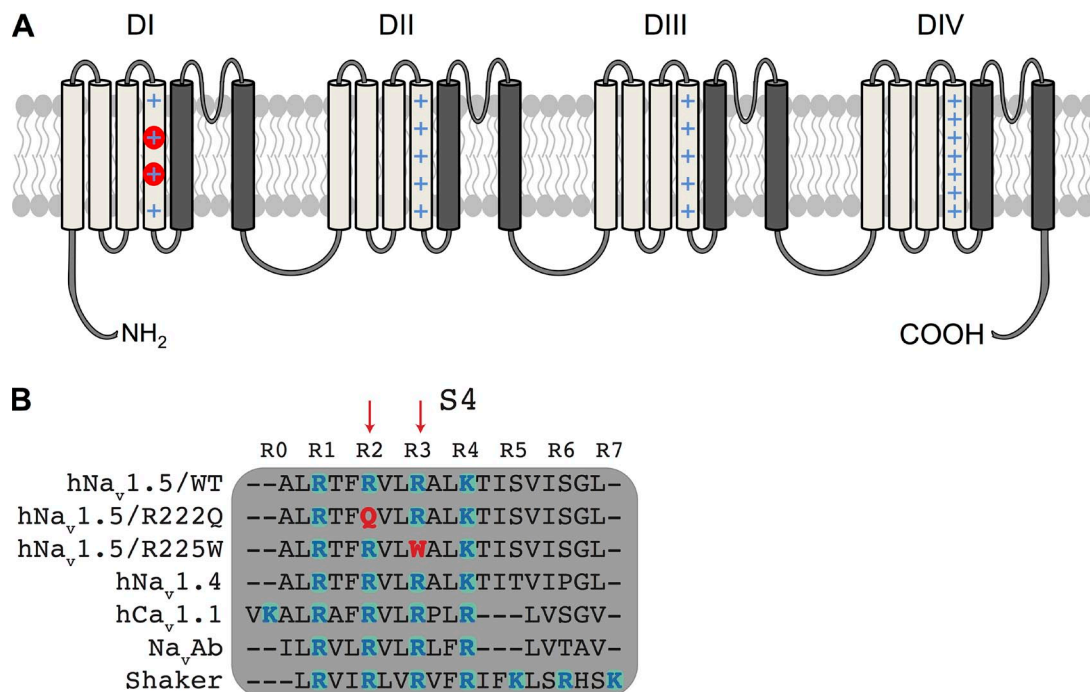www.jgp.org/cgi/doi/10.1085/jgp.201411304

93

Figure 1. The R222Q residue is highly conserved among ion channels. (A) Schematic 2-D representation of the 24-transmembrane segments of Na$_v$1.5 organized in four homologous domains. The red circles indicate the locations of the R222Q and R225W mutations. (B) The S4 segments of the first domains of the Na$_v$1.5, Na$_v$1.4, and Ca$_v$1.1 channels, and the S4 segments of the Na$_v$Ab and Shaker channels were aligned using CLC sequence viewer 6 (QIAGEN). Positively charge residues (arginines or lysines) are numbered from R0 to R7 and bolded in blue. The R2 and R3 indicated by the red arrow correspond to R222Q and R225W in Na$_v$1.5.

propose that the gating pore currents induced by these mutations contribute to the atypical phenotype that associates complex arrhythmias and cardiac dilatation.

MATERIALS AND METHODS

Cell culture

The electrophysiological experiments were conducted using tsA201 cells, which are modified human embryonic kidney HEK-293 cells stably transfected with simian virus 40 large T antigen. The cells were cultured in high glucose Dulbecco's modified Eagle's medium supplemented with 10% FBS, 2 mM L-glutamine, 100 U/ml penicillin G, and 10 mg/ml streptomycin (Gibco) at 37°C in a 5% CO$_2$ humidified atmosphere. They were transfected with WT or mutant Na$_v$1.5 cDNA (5 µg) using the calcium phosphate method as described previously (Deschênes et al., 2000). The Na$_v$1.5 α subunit was cotransfected with the β1 subunit. In brief, 5 µg of each cDNA was mixed with 500 µl of a 250-mM CaCl$_2$ solution to which 500 µl HeBS2x (0.28 M NaCl, 0.05 M HEPES, and 1.5 M Na$_2$HPO$_4$) was added.

Patch-clamp recordings

Macroscopic Na$^+$ currents (α currents) were recorded at room temperature 48–72 h after transfection using the whole-cell configuration of the patch-clamp technique as described previously (Huang et al., 2011). The liquid junction potential between the patch pipette and the bath solution was not corrected. P/4 leak subtraction was used for the α pore current recordings but was not used for the gating pore current recordings. However, for the gating pore currents, offline linear leak subtraction at hyperpolarized voltages was performed to eliminate inherent nonspecific leaks. Currents were recorded with a sampling rate of 83.33 kHz

and were low-pass filtered at 5 kHz. The estimation of the unitary conductance of the gating pore currents was based on Ohm's law, assuming that the Na$_v$1.5 unitary conductance was 22 pS (Gellens et al., 1992) and that the maximum open probability of the gating pore occurred at 40 mV.

Solutions

The compositions of intrapipette and bath solutions used to record the whole-cell α Na$^+$ currents and gating pore currents are described in Table 1. The pHs of all the solutions were adjusted to 7.4 using methanethiosulfonic acid and CsOH, NaOH, or KOH as required. The bath solutions contained 10 mM TEA-Cl to block endogenous potassium currents. 1 mM niflumic acid freshly prepared in 100% ethanol was added to the bath solution before recording the gating pore currents to block endogenous chloride channels. When indicated, 10 µM tetrodotoxin (TTX; Latoxan) was added to the bath solution to block α pore current.

Sequence alignment and homology modeling of the activated state

The procedure was similar to the one described in Gosselin-Badaroudine et al. (2012a). The best available template to build a model of the activated state of the DI VSD of the Na$_v$1.4 channel was identified by a PSI-BLAST search of the Protein Data Bank (PDB) database. We selected the Na$_v$Ab high resolution structure released in 2011 (Payandeh et al., 2011) because it bears the transmembrane domains with the highest max score. To build the pairwise alignment between Na$_v$1.5 and Na$_v$Ab, the first 100 human homologous sequences to Na$_v$Ab in the National Center for Biotechnology Information reference protein database, which includes Na$_v$1.5, were identified using the PSI-BLAST server. A multiple sequence alignment of the 100 sequences was constructed using the ClustalW2 online server (Larkin et al., 2007). The BLOSUM

protein weight matrix was used together with standard parameters (opening gap penalty of 10, gap extension penalty of 0.20, and gap distance of 5). The pairwise alignment of Na_vAb and $Na_v1.5$ was extracted and used to build a 3-D atomistic model of the mammalian channels. The alignment of the VSD transmembrane segments used for the structural modeling is presented in Fig. S1. A standard MODELLER (Eswar et al., 2006) routine was then used to build a comparative model of the DI VSD of the $Na_v1.5$ channel. Because the S3 of Na_vAb was surprisingly short and because the transmembrane topology prediction software predicted that the S3 helix of the DI of the $Na_v1.5$ channel extended to residue 212, we imposed helicity in our modeler routine.

Sequence alignment and homology modeling of alternate VSD states

The activation/deactivation mechanism of the voltage sensor of voltage-gated ion channels is thought to proceed in a stepwise manner and involves a sliding of the S4 helix relative to a rather static S1–S3 bundle (outward/inward, respectively) (Delemotte et al., 2011; Amaral et al., 2012; Gosselin-Badaroudine et al., 2012a; Henrion et al., 2012; Jensen et al., 2012; Lacroix et al., 2012; Vargas et al., 2012; Yarov-Yarovoy et al., 2012). Each state is believed to be stabilized by several transmembrane salt bridges between S4 gating charges and negative charges provided by the S1–S3 glutamic and aspartic residues and the lipid head group phosphate moieties. During deactivation, the transitions between consecutive states involve a downward ratchet-like movement of S4 in which each of the S4 charges jumps from a negatively charged binding site to the next. This arrangement of positive S4 amino acids and negative S1–S3 charges has been identified as the gating charge transfer center (GCTC) (Tao et al., 2010). Together, S1–S3 segments strongly interact with the S4 segment, thus stabilizing its position either during its transitions or in its resting and activated conformations where R1 and K4 are, respectively, located in the GCTC (Lin et al., 2011; Schwaiger et al., 2012; Gamal El-Din et al., 2013; Lacroix et al., 2014; Moreau et al., 2014b).

To produce models of alternate states of the DI VSD of the $Na_v1.5$ channel, we used a procedure similar to the one described in Wood et al. (2012) used to produce models of two different states of the proton voltage-gated ion channel H_v1. Building an alignment in which S4 is manually shifted by three residues toward the N terminus (corresponding to one helical turn; see Fig. S1) produced a homology model of an intermediate state downward of α, that we call β, using the nomenclature proposed in previous work (Delemotte et al., 2011; Gosselin-Badaroudine et al., 2012a). Producing another alignment in which S4 is manually shifted by

six residues relative to the original alignment produced another intermediate state further along deactivation, called γ.

Note that this procedure results in states that are more stable than the steered molecular dynamics procedure devised earlier by our group (Delemotte et al., 2011; Amaral et al., 2012; Gosselin-Badaroudine et al., 2012a).

Molecular dynamic simulations

The three states of the DI VSD of $Na_v1.5$ were then inserted in a fully hydrated 1-palmitoyl-2-oleoyl-sn-glycero-3-phosphocholine bilayer. The systems were equilibrated under normal constant temperature and pressure conditions (298°K, 1 atm.) in a 150-mM NaCl solution. The lipid tails were melted during the first nanosecond, restraining the position of the protein, lipid head groups, water molecules, and ions to their initial position with a strong harmonic potential. To ensure correct reorganization of the lipids and solution, the positions of all the atoms of the channel were then restrained for 2 ns. The side chains were then allowed to reorganize while the backbone was kept restrained for 8 ns. Lastly, a 100-ns unrestrained molecular dynamics simulation of the entire system was conducted, enabling the system to relax. The molecular dynamics simulations were performed using the NAMD2 program (Phillips et al., 2005). Langevin dynamics were applied to keep the temperature (300°K) fixed. The equations of motion were integrated using a multiple time-step algorithm (Izaguirre et al., 1999). Short- and long-range forces were calculated every one and two time steps, respectively, with a time step of 2.0 fs. Chemical bonds between hydrogen and heavy atoms were constrained to their equilibrium value. Long-range electrostatic forces were taken into account using the particle mesh Ewald approach (Darden et al., 1993). The water molecules were described using the TIP3P model (Jorgensen et al., 1983). The simulation used the CHARMM22-CMAP force field with torsional cross-terms for the protein (MacKerell et al., 1998, 2004) and CHARMM36 for the phospholipids (Feller and MacKerrell, 2000). The simulations were performed on the CRAY XT5 KRAKEN at the National Institute for Computer Science and on Owlsnest, Temple University's supercomputing facility.

Data analysis and statistics

The electrophysiological data were analyzed using Clampfit (pCLAMP v10.0; Molecular Devices) and custom-written MATLAB programs (The MathWorks Inc.). Data are expressed as means ± SEM. When indicated, a t test was performed using SigmaPlot software (Jandel Scientific Software). Differences were considered significant at a $P < 0.05$ (*), < 0.01 (**), or < 0.001 (***).

TABLE 1

Compositions of solutions

	Intrapipette								Bath					
	1		2		3		4			5		6		7	
CsF	135	KF	135	NaF	130	NMDG-F	130		NMDG	115	NMDG	115	NMDG	135
NaCl	5	NaCl	5	NaCl	5	NaCl	5		NaCl	20	NaCl	20	NaCl	2
EGTA	10	EGTA	10	EGTA	10	EGTA	10		CsCl	2	KCl	2	$Ca(OH)_2$	2
HEPES	10	HEPES	10	HEPES	20	HEPES	10		$Ca(OH)_2$	2	$Ca(OH)_2$	2	TEA-Cl	10
									HEPES	10	HEPES	10	HEPES	20
									TEA-Cl	10	TEA-Cl	10	Nif	1
									Nif	1	Nif	1		

(Solutions 1–7) Compositions of the intrapipette and bath solutions (mM) used to record whole-cell Na^+ currents (1, 5) and gating pore currents (1–7). Solutions 1 and 5 were used to record gating pore current selective for Cs^+. Solutions 2 and 6 were used to record gating pore currents selective for K^+. Solutions 3 and 7 were used to record gating pore currents selective for Na^+. Solutions 4 and 5 were used to evaluate the permeation of NMDG. $Ca(OH)_2$, calcium hydroxide; $CaCl_2$, calcium chloride; CsF, cesium fluoride; EGTA, ethylene glycol tetra acetic; KCl, potassium chloride; $MgCl_2$, magnesium chloride; NaCl, sodium chloride; Nif, niflumic acid; NMDG(-F), N-methyl-ᴅ-glucamine (fluoride); TEA-Cl, tetraethyl ammonium chloride.
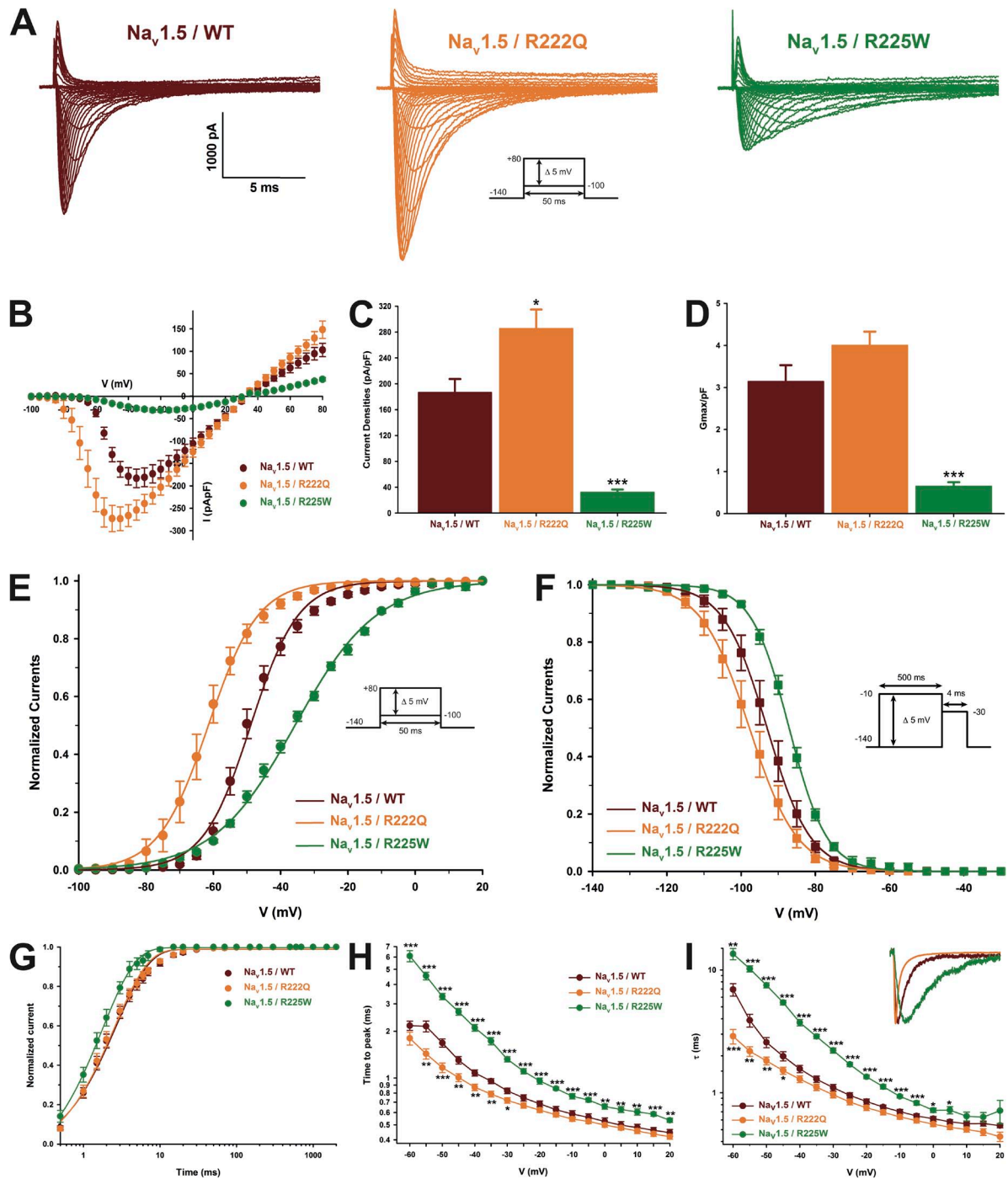
Figure 2. Biophysical characterization of the $Na_v1.5$ mutant channels. The results for the $Na_v1.5$ WT channel are indicated by red symbols, those for the R222Q mutant channel by orange symbols, and those for the R225W mutant channel by green symbols. (A) Representative whole-cell current traces of the WT and mutant channels. Currents were elicited using a voltage-clamp protocol where depolarizing pulses were applied for 50 ms from −100 to 80 mV in 5-mV increments (see protocol in inset). (B) Current density–voltage (I-V) relationships of the WT and mutant channels. (C) Histogram summarizing the peak current density of the WT and mutant channels. The R222Q channel displayed a higher peak current density than the WT channel (−285.5 ± 29.4 pA/pF, $n = 13$, and −186.5 ± 21.0 pA/pF, $n = 9$, respectively). The R225W mutation reduced the peak current density (−32.3 ± 4.2 pA/pF, $n = 11$). (D) The maximal global conductance (G_{max}) of each cell was normalized to the cell membrane capacitance. No differences were observed between the WT (3.1 ± 0.4 pS/pF, $n = 9$) and R222Q channels (4.0 ± 0.3 pS/pF, $n = 13$), indicating that there were a similar number of each type of channel on the cell surface. On the other hand, the normalized conductance was significantly lower for the R225W channel (0.6 ± 0.1 pS/pF, $n = 11$), indicating that there were fewer R225W channels in the cell membrane. (E) Voltage dependence of steady-state activation of the WT and mutant channels. Activation curves were generated using a standard Boltzmann distribution ($G(V)/G$max $= 1/(1 + \exp(−(V − V_{1/2})/k)))$ to give the $V_{1/2}$ and k values listed in Table 2. (F) Steady-state inactivation of the WT and mutant channels. Inactivation currents

Biophysical parameters	WT ($n = 9$)	R222Q ($n = 13$)	R225W ($n = 11$)
Peak Current (pA/pF)	-186.5 ± 21.0	-285.5 ± 29.4^a	-32.3 ± 4.2^b
Normalized G$_{max}$ (pS/pF)	3.1 ± 0.4	4.0 ± 0.3	$0.6 \pm 0.1b$
Activation			
V$_{1/2}$ (mV)	-48.9 ± 1.3	-61.8 ± 2.1^b	-37.0 ± 1.1^b
k (mV)	-6.6 ± 0.5	-5.7 ± 0.5	-12.0 ± 0.3^b
Inactivation			
V$_{1/2}$ (mV)	-93.2 ± 1.7	-97.8 ± 2.0	-89.3 ± 0.9^a
k (mV)	5.0 ± 0.2	4.8 ± 0.1	5.4 ± 0.3
Recovery from inactivation			
τ (ms)	3.2 ± 0.3	3.1 ± 0.3	2.4 ± 0.2^a
Peak ramp current (% peak current)	-2.7 ± 0.3	-4.2 ± 0.5^a	-9.4 ± 0.5^b
Peak ramp current (pA/pF)	-4.6 ± 0.8	-12.7 ± 2.7^a	-2.3 ± 0.3^a

V$_{1/2}$, midpoint for activation or inactivation; k, slow factor for activation or inactivation. For all values, $n > 6$.
[a]Difference between Na$_v$1.5/WT; P < 0.05.
[b]P < 0.001.

Online supplemental material

In Fig. S1, the alignment used to build homology models of the alternate α, β, and γ states of the VSD is shown. In Fig. S2, the water density profiles along the main axis of the VSD in the WT and mutant channels is shown. In Fig. S3, a proposed pathological mechanism related to the presence of a gating pore current is shown. The published biophysical characteristics and clinical phenotypes associated to the R222Q and R225W mutations are shown in Table S1. The salt-bridge patterns in the different models are summarized in Table S2. The PDB files of each model are also available for download as a ZIP file. The online supplemental material is available at http://www.jgp.org/cgi/content/full/jgp.201411304/DC1.

RESULTS

The R222Q and R225W mutations induce divergent biophysical properties

The classical biophysical characterization of the mutant channels revealed that the R222Q mutation slightly increased the peak current density, whereas the R225W mutation markedly reduces it (Table 2 and Fig. 2). However, the maximal normalized conductance (G$_{max}$/pF) of the R222Q channel did not increase significantly, indicating that the cell surface channel density was not affected (Fig. 2). The two mutations produced opposite shifts in steady-state activation and inactivation (Fig. 2). The recovery from inactivation was not affected by the R222Q mutation, whereas it was significantly faster for the R225W mutation (Table 2 and Fig. 2). The time to peak and the current decay were both faster for the R222Q channel and slower for the R225W channel than for the WT channel (Fig. 2). Lastly, when normalized to the peak current, the ramp current was higher for both mutations (Fig. 3), although it exhibited different voltage dependence.

The Na$_v$1.5 R222Q and R225W mutant channels conduct a gating pore current at depolarized voltages

The nature of the R to Q or W mutation and their spatial localization on the Na$_v$1.5 protein (Fig. 1, R2, R3, respectively; S4/DI) prompted us to examine the possible existence of a gating pore current through the mutant channels. We recorded nonleak-subtracted currents induced by 80-ms voltage steps from −100 to 40 mV. Fig. 4 shows examples of raw data of WT and mutant channel gating pore currents recorded in Cs$^+$ solutions. The corresponding offline linear leak subtraction showed that a nonlinear component appears on the mutant channels but not on the WT channel (Fig. 4 A, bottom traces). After an offline subtraction of the linear leak, the gating pore currents were normalized to the cell capacitance to obtain the gating pore current density–voltage relationships for the WT and mutant channels

were obtained by applying conditioning prepulses to membrane potentials ranging from a holding potential of −140 to −10 mV for 500 ms in 5-mV increments and were then measured using a 4-ms pulse to −30 mV at each step (see protocol in inset). The recorded inactivation values were fitted to a standard Boltzmann equation ($I(V)/I$max = $1/(1 + \exp((V - V_{1/2})/k)) + C$) to give the values listed in Table 1. (G) Recovery from fast inactivation was obtained using a two-pulse protocol at 30 mV to obtain maximal activation (see protocol in inset). The time constants listed in Table 1 were obtained using a two-exponential function: ($A_{fast}(1 - \exp(-t/\tau_{fast})) + A_{slow}(1 - \exp(-t/\tau_{slow})) + C$). (H) The times to peak of the WT and mutant channels were used to evaluate the activation kinetics. The times to peak were measured on the same current traces used to construct the I-V relationship. (I) The time constants of fast inactivation decay were plotted as a function of voltage for the WT and mutant channels. The time constants were obtained using a simple-exponential function: ($A_{fast}(\exp(-t/\tau) + C$). Normalized raw data shown in the inset illustrate the current decay kinetics. Data are expressed as means ± SEM. Differences were considered significant at P < 0.05 (*), < 0.01 (**), or < 0.001 (***).

(Fig. 4 B). These gating pore currents were also recorded in the presence of 10 µM TTX to completely block the central pore (Fig. 4 B). The resulting gating pore currents were indistinguishable from traces without TTX, demonstrating that the current does not flow through the usual α pore of the protein. Fig. 4 C shows the normalized voltage dependence of gating pores based on the theoretical reversal potential of Cs^+ in the recordings solutions. The R222Q and R225W mutations show a $V_{1/2}$ of 1.2 ± 3.7 mV (n = 7) and 13.5 ± 5.7 mV (n = 7), and a slope factor of −19.0 ± 1.7 mV (n = 7) and −15.1 ± 2.2 mV (n = 7), respectively. The gating pore current density at 40 mV was larger for the R222Q mutant (6.6 ± 1.0 pA/pF, n = 8, without TTX and 6.7 ± 0.6 pA/pF, n = 7, with TTX) than for the WT channel (0.17 ± 0.09 pA/pF, n = 5) and R225W mutant (2.7 ± 0.3 pA/pF, n = 10, without TTX and 2.4 ± 0.4 pA/pF, n = 6, with TTX) channels (Fig. 4 D). The α current at −10-mV and the gating pore current at 40-mV relationship is shown Fig. 4 E. A linear correlation was found (r^2 = 0.85 for R222Q channels and r^2 = 0.86 for R225W channels), indicating that the amplitude of gating pore currents is correlated to the amplitude of the α pore current. The gating pore created by the mutations allowed the passage of K^+, Cs^+, and Na^+ ions while it excludes the passage of $NMDG^+$ (Fig. 5). Correction for the electrochemical gradient yielded the relative permeation for the ions. The gating pores of the two mutations were less permeable to K^+ and Na^+ than to Cs^+, whereas no permeation was found with $NMDG^+$ (Fig. 5). Indeed, the relative permeability of the mutant channels was approximately two times higher for Cs^+ than for K^+ (2.2 ± 0.3 for the R222Q channel and 2.0 ± 0.2 for the R225W channel) (Fig. 5 C), whereas the relative permeability of Na^+ was lower than for K^+ (0.59 ± 0.08 for the R222Q channel and 0.67 ± 0.05 for the R225W channel; Fig. 5 C).

It was recently proposed that arginine mutations inside the VSD would cause a loss of mobility (or a partial freezing) of the S4 after long depolarization periods (Sokolov et al., 2008; Fan et al., 2013; Groome et al., 2014). In the presence of 10 µM TTX, a 500-ms predepolarization was used to mimic the cardiac AP duration. We then applied a ramp protocol from −140 to 0 mV at 0.72 mV/ms to measure gating pore current (see protocol in inset of Fig. 6). At hyperpolarized potentials, gating pore currents were observed after a long depolarization for both R222Q and R225W mutations (−5.6 ± 1.1 pA/pF, n = 5, for R222Q and −3.3 ± 0.6, n = 3, for R225W) and were absent for the WT (−0.9 ± 0.1 pA/pF, n = 5). Such currents could not be
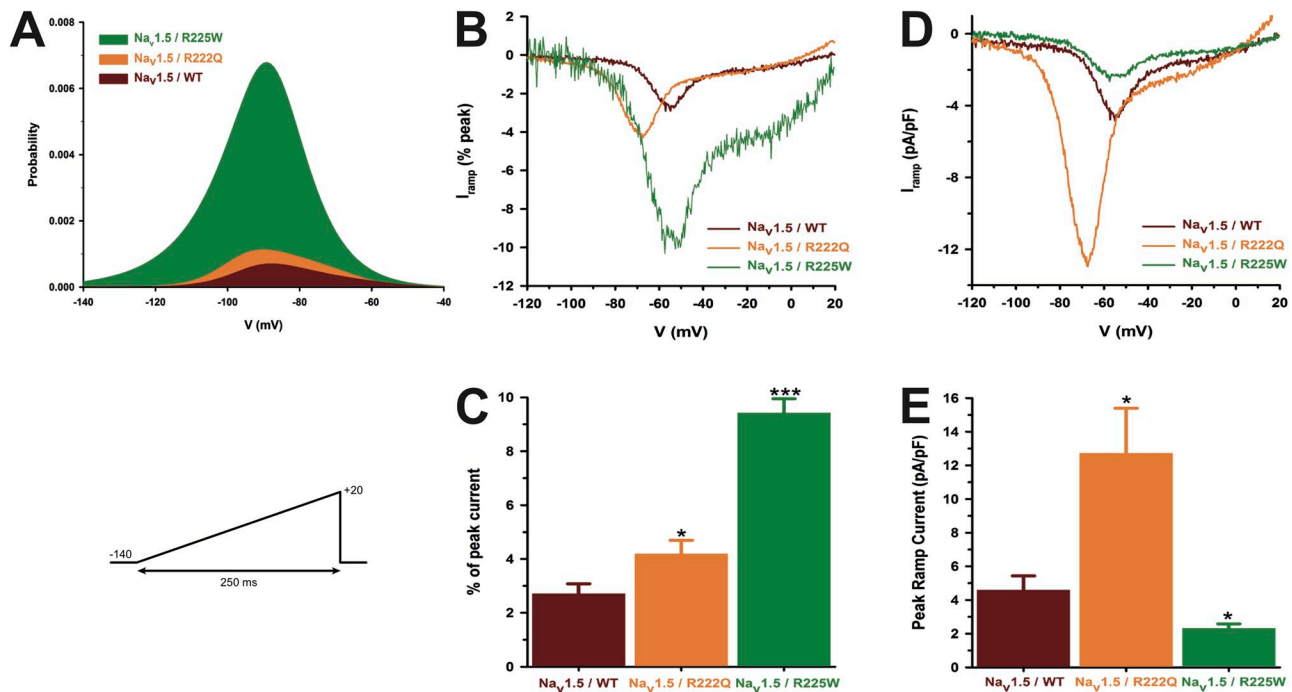

Figure 3. Window currents of the Na$_v$1.5 WT and mutant channels. (A) The overlap between activation and inactivation defines the window current. The predicted window current was obtained using the following equation: $(1/(1 + \exp((V_{1/2activation} - V)/k_{activation}))((1 - C)/(1 + \exp((V - V_{1/2inactivation})/k_{inactivation})) + C)$. The presence of the mutation increased the predicted window current over 2.3-fold. (B–E) Ramp protocols (see protocol in inset) were imposed (0.64 mV/ms) to study the window current. As predicted in A, the window currents of the mutant channels were higher than that of the WT channel. (B) Ramp current traces normalized to the α peak current. (C) Histogram showing the peak window current normalized to the α peak current (% of peak current). (D) Average traces of ramp currents normalized to cell capacitance to study ramp current density. (E) Peak ramp current density (pA/pF). Data are expressed as means ± SEM. Differences were considered significant at P < 0.05 (*) or < 0.001 (***).

observed without the 500-ms predepolarization (Fig. 6). These results show that after long depolarization periods, the mutated S4 segments need more time to resume their resting position and thus partially remain in a conformation, likely enabling gating pore current conduction.

Structural models of the Na$_v$1.5 DI VSD reveal that the R222Q and R225W mutations open an alternative permeation pathway

To gain a better molecular insight into the effect of the mutations, we constructed homology models of the Na$_v$1.5 VSD using the high resolution structure of the
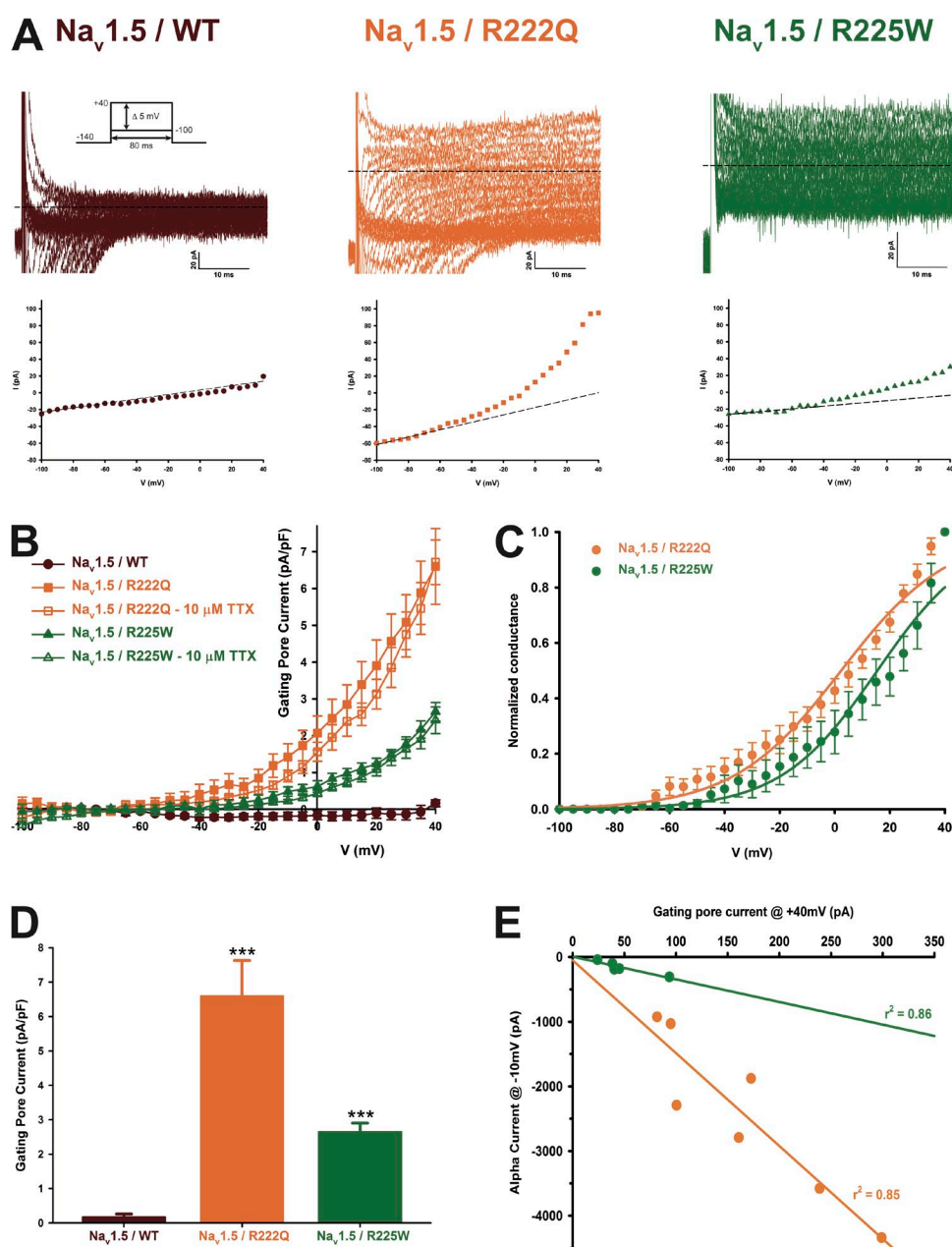

Figure 4. The Na$_v$1.5 R222Q and R225W channels conduct gating pore currents. Gating pore currents were recorded using a voltage-step protocol from -100 to 40 mV in 5-mV increments. (A) Examples of raw traces of gating pore currents recorded in Cs$^+$ solutions (solutions 1 and 5 in Table 1). The inward α pore current is not totally shown for WT and R222Q channels. For R225W channels, this current is mingled in the gating pore current traces as a result of lower channel expression. The currents are also plotted as a function of voltage at the bottom of each trace. Linear nonspecific leaks are indicated by dotted lines. (B) Current density–voltage relationships of gating pore currents recorded for the WT, R222Q, and R225W channels in the absence of TTX are shown in closed symbols (n = 8 for R222Q, n = 10 for R225W, and n = 5 for WT channels). The current density–voltage relationships in the presence of 10 µM TTX are shown in open symbols (n = 7 for R222Q and n = 6 for R225W channels). (C) Normalized voltage dependence of gating pore currents caused by R222Q and R225W mutations. Curves were fitted using a standard Boltzmann distribution (*Normalized conductance* = $1/(1 + \exp(-(V - V_{1/2})/k))$). (D) Histogram summarizing the gating pore current densities at 40 mV in a Cs$^+$ solution for the WT, R222Q, and R225W channels (0.17 ± 0.09 pA/pF, 6.6 ± 1.0 pA/pF, and 2.7 ± 0.3 pA/pF, n = 5–10). (E) Coupling between the α pore and the gating pore current. Each point represents the α peak current amplitude at -10 mV and the associated gating pore current amplitude at 40 mV. Lines indicate the best linear regression and the associated r^2 Data are expressed as means ± SEM. Differences were considered significant at P < 0.001 (***).
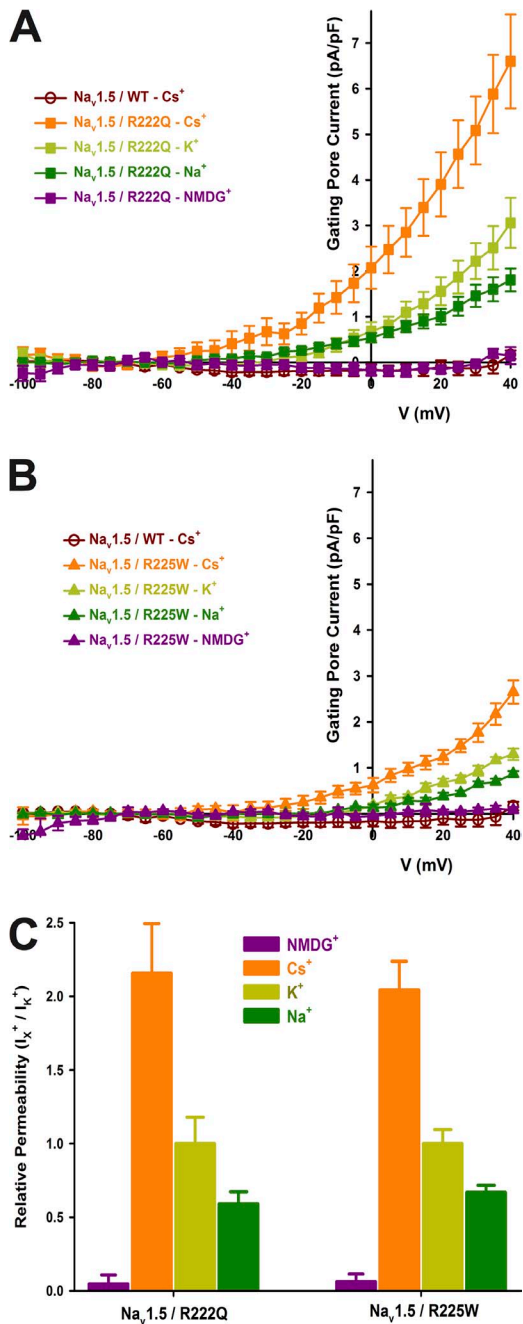
Figure 5. Gating pore current ionic selectivity. After linear leak subtraction, the gating pore currents were normalized to the cell capacitance and plotted as a function of voltage. The WT channel displayed an almost nonexistent gating pore current of 0.17 ± 0.09 pA/pF ($n = 5$). The solution used to record gating pore are listed in Table 1 (solutions 1 and 5 for Cs^+ condition, solutions 2 and 6 for K^+ condition, solutions 3 and 7 for Na^+ condition, and solutions 4 and 5 for $NMDG^+$ condition). (A) The normalized gating pore current carried by Cs^+ was 6.6 ± 1.0 pA/pF ($n = 8$), the maximal K^+ current was 3.1 ± 0.5 pA/pF ($n = 7$), and the maximal Na^+ current was 1.8 ± 0.3 pA/pF ($n = 8$) for the R222Q channel. No $NMDG^+$ currents were observed (0.1 ± 0.2 pA/pF, $n = 4$). (B) The normalized gating pore current carried by Cs^+ was 2.7 ± 0.3 pA/pF ($n = 10$), the maximal K^+ current was 1.3 ± 0.1 pA/pF ($n = 4$), and the maximal Na^+ current was 0.87 ± 0.06 pA/pF ($n = 5$) for the R225W channel. No $NMDG^+$ currents were observed

partially activated state of Na_vAb (Payandeh et al., 2011) as a template. We used three alternate alignments in the S4 region (Fig. S1) to build models of three different states (α, β, and γ, with α being the most activated).

As reported previously, the solvent-accessible volume in the four-helix VSD has an hourglass shape in all three states (Fig. 7) (Treptow and Tarek, 2006; Jogini and Roux, 2007; Krepkiy et al., 2009; Delemotte et al., 2010; Ramsey et al., 2010; Gosselin-Badaroudine et al., 2012a; Wood et al., 2012; Li et al., 2014). In each state, a single S4 charge that is located in the constricted region in the center of the VSD, R228 in α, R225 in β, and R222 in γ (Table S2). In the WT models, water density profiles (Fig. S2, dark blue and red lines) indicated that water protrudes from both sides of the membrane, defining two crevices separated by a thin hydrophobic septum. The septum is indicated by a local number density <1.0 located around the conserved aromatic tyrosine at position 168 on S2.

The introduction of the R222Q mutation in the γ state and the R225W mutation in the β state disrupted the salt bridge connecting these residues. This leads to a swelling of the four-helix bundle and the appearance of a solvated pathway through the VSD (Fig. 7). Notably, the R225W mutation opened up a wider hydrophilic funnel than the R222Q mutation (Figs. 7 and S2), potentially accounting for the higher gating pore conductance in this mutant.

DISCUSSION

We hypothesized previously that the gating pore current might be a potential pathological mechanism in the development of complex arrhythmias associated with cardiac dilatation (Gosselin-Badaroudine et al., 2012b, 2014; Moreau et al., 2014a). Several $Na_v1.5$ mutations, including R222Q and R225W, have been reported to be associated with very similar clinical phenotypes. However, there is no consensus on the biophysical defects induced by these mutations. Also, the possibility that these two mutations might generate gating pore currents has never been investigated (Table S1). Here, we report that the R222Q and R225W mutant channels have divergent biophysical properties, which is in agreement with previously published results. No persistent current was observed for both mutant channels (not depicted). Similar mutations are usually associated with pure electrical disorders such

(0.1 ± 0.1 pA/pF, $n = 4$). (C) Histogram summarizing the relative permeabilities of the gating pore currents. Cs^+ was approximately twice as permeant as K^+ (2.2 ± 0.3 for the R222Q channel and 2.0 ± 0.2 for the R225W channel). Na^+ was less permeant than K^+ (0.59 ± 0.08 for the R222Q channel and 0.67 ± 0.05 for the R225W channel). $NMDG^+$ was dramatically less permeant than K^+ (0.05 ± 0.06 for R222Q channel and 0.06 ± 0.05 for R225W channel). Data are expressed as means $\pm$ SEM.

as type 3 long QT syndrome and Brugada syndrome (Ruan et al., 2009). However, the clinical phenotypes associated with these mutations are clearly atypical and are probably not caused only by the gain or loss of channel function. Furthermore, such an opposite gain and loss of channel function mechanism has never been associated to identical clinical phenotype. The hypothesis of arrhythmia-induced dilatation has been discarded because of the young age (1-yr-old) patient carrying the R225W mutation (Bezzina and Remme, 2008). Physiologically, both mutations are expected to impact the integrity of the AP in cardiomyocytes. Indeed, both R222Q and R225W mutations have an important impact on the biophysical properties of the α pore of Na$_v$1.5 mutated channels. The gain of function of the R222Q mutant channels would probably favor the premature initiation of AP, notably by increasing the Na$^+$ entry through the α pore (caused by shifts in both activation and inactivation), which increases the depolarizing currents especially at hyperpolarized voltages where WT channels are expected to be closed. The premature ventricular contractions usually observed

in patients carrying this mutation strengthen this hypothesis (Laurent et al., 2012; Mann et al., 2012). In contrast, the loss of function of R225W mutant channels caused by reduced membrane expression and shifts in both activation and inactivation would decrease the ability of mutated channels to initiate APs. This would be the cause of atrio-ventricular blocks shown in patients carrying the R225W mutation (Bezzina et al., 2003). Consequently, although both mutations induce divergent biophysical defects, each defect could potentially explain some pathological phenotype aspects. However, even if the impact of the defective α pore cannot be denied, the complexity and the similarity of the pathological phenotypes would probably not be only related to these divergent biophysical defects.

Our results revealed that under depolarized conditions, a new permeation pathway different from the α pore is created. Indeed, similar currents were recorded with or without TTX. These gating pores are selective for larger cations, as shown by their relative permeability (Fig. 5). The gating pore caused by the R222Q mutation
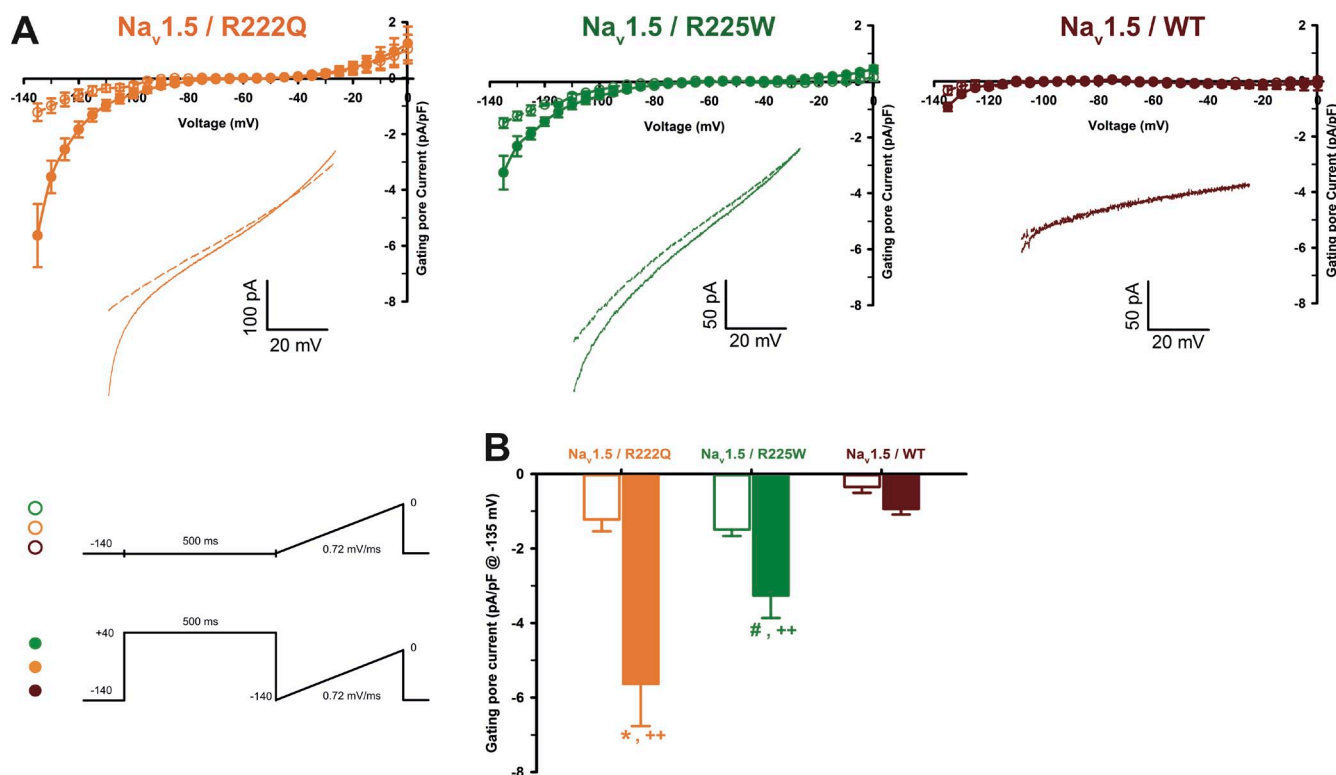

Figure 6. Gating pore current after long depolarizations. (A) Current generated by ramp pulses (see protocols in inset), for R222Q (left), R225W (middle), and WT (right) channels (using solutions 1 and 5 listed in Table 1). The I-V curves were constructed by averaging values of current at each 5 mV. The voltage was calculated using the known time course of the ramp protocol. Thus, for purpose of clarity, the plotted points (mean ± SEM) do not represent steady-state currents, but they represent average current every 5 mV. The linear leak subtraction around −75 to −45 mV was performed to eliminate inherent linear leak. The insets show the currents in response to ramp protocols. Dashed lines indicate the current obtained without 500-ms predepolarization. Solid lines indicate the response after 500-ms predepolarization. (B) Histogram summarizing the inward gating pore current density at −135 mV recorded with or without 500-ms predepolarization. R222Q and R225W exhibit gating pore currents when compared with control ramp protocols without predepolarization (−5.6 ± 1.1 pA/pF, n = 5, for R222Q [*], and −3.3 ± 0.6, n = 3, for R225W [#]). ++, statistical difference between mutant and WT condition (P < 0.01). Data are expressed as means ± SEM. Differences were considered significant at P < 0.05 (*, #) or < 0.01 (++).

activates at less positive potentials than the one caused by the R225W mutation, as shown in Fig. 4 C. These cation leak currents are essentially a gain of function, as they induce a cation leakage that is not present when an arginine occupies the 222 or 225 position. Using Ohm's law, the unitary conductance of the gating pore was estimated at 72 fS for the R222Q mutant and 126 fS for the R225W mutant, raising the intriguing possibility that the perturbation induced by the R225W mutation is more marked. Indeed, our structural model also provided a molecular explanation for the increased conductance. The increased hydrophobic nature of the tryptophan causes this residue to bury its side chain in the S3–S4–lipid tail interface, twisting slightly the bottom of S4 (counterclockwise when looking from the bottom), whereas glutamine remains preferentially oriented toward the hydrophilic pore (Fig. 7). This leads to the opening of a wider hydrophilic pore throughout the VSD in R225W (as shown Fig. S2). As we suggested previously (Gosselin-Badaroudine et al., 2014; Moreau et al., 2014a), the resulting gating pore current might be a common biophysical defect of the R222Q and R225W mutant channels.

Both R222Q and R225W mutations impact the channel activation and inactivation process, denoting an effect on the voltage-sensing mechanism of the mutated S4 segment. Interestingly, the published data about S4 arginine neutralization indicate a wide variability of the impact of such neutralization on the α pore gating (Chahine et al., 2004; Blanchet and Chahine, 2007; Miceli et al.,

2008, 2012; Sokolov et al., 2008; Berger and Isacoff, 2011; Gosselin-Badaroudine et al., 2012b). Given the crucial role of arginines in the voltage-sensing mechanism, it can be expected that their neutralization would impair the S4 movement and thus induce a depolarizing shift of the activation. It is also important to note that the α pore channel opening might be dependent on the S4 movement but also on the coupling between the VSD and the pore. The absence of effect on channel activation observed with several mutations such as R669Q/W (R3) on Na$_v$1.4 DII (Sokolov et al., 2008) might denote their little impact on the S4-sensing mechanism (and that the VSD can be adequately coupled to the α pore of the channel). Oppositely, impacts on channel gating of R222Q and R225W mutations might indicate that either the sensing mechanism or the coupling with the α pore of mutant channels is affected. Finally, such discrepancies on the effect of S4 neutralization could also be a marker of structural differences between channel VSDs. Indeed, although VSDs are composed of similar motifs (positives charges on the S4, the presence of a GCTC in S1–S3), each VSD possesses its own biophysical characteristics and thus its own structural identity.

Gating pores have been associated with the development of periodic paralyses (Sokolov et al., 2007, 2008; Struyk and Cannon, 2007; Moreau et al., 2014a). Periodic paralyses are caused by arginine mutations in S4 of Ca$_v$1.1 or Na$_v$1.4, the skeletal muscle homologue of Na$_v$1.5. Interestingly, the Na$_v$1.4 R222W mutation (R2 of DI of S4) has been associated with the development
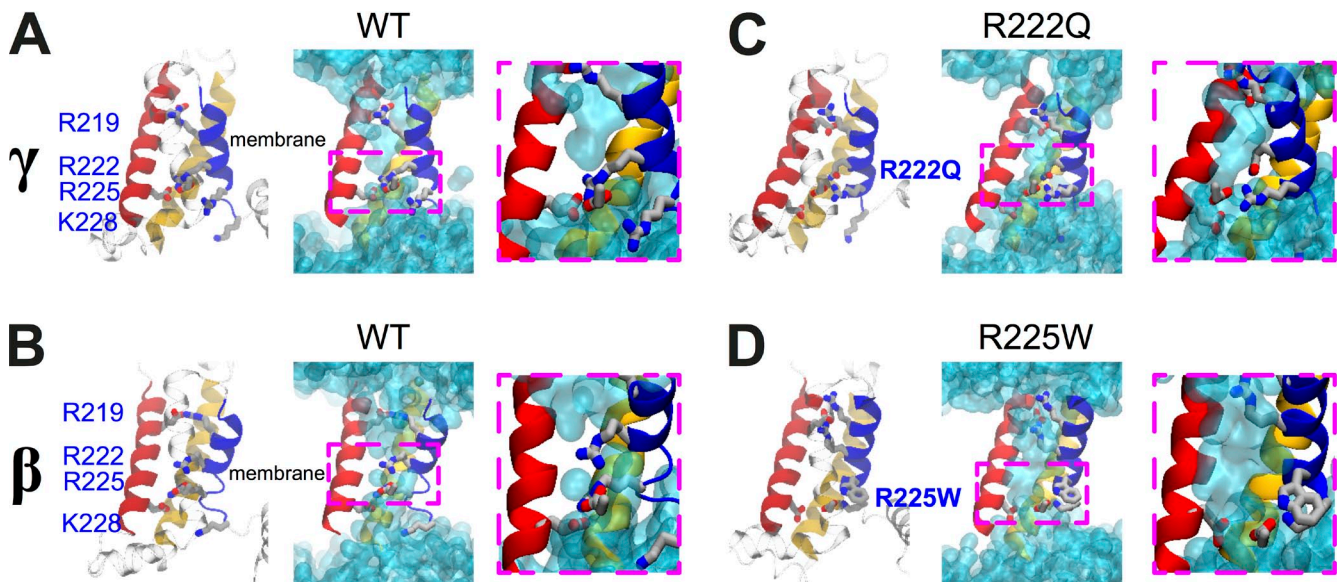

Figure 7. Structural models of the DI VSDs of the Na$_v$1.5 WT, R222Q, and R225W mutants. Structural models of the relaxed DI VSD of the WT in the γ (A) and β (B) states. (C) Structural model of the relaxed DI VSD of the R222Q mutant in the γ state. (D) Structural model of the relaxed DI VSD of the R225W mutant in the β state. For all the structural models, the VSD protein backbone is represented as a ribbon (left panel, S1 in yellow, S2 in red, S3 in transparent cyan, and S4 in blue). The gating charges of S4 and the counter charges of S2 and S3 are shown as sticks (carbon in gray, nitrogen in blue, and oxygen in red; hydrogens are omitted for clarity). In the middle panel, the water-accessible volume is shown as a transparent cyan surface. For each configuration, a higher magnification of the GCTC (dotted pink box) is shown.

of hypokalemic periodic paralysis (HypoPP) (Matthews et al., 2009; Park and Kim, 2010).

The properties of two HypoPP mouse models also lend credence to the association between the gating pore and the development of HypoPP. These two models also present a dilatation of transverse tubules, indicating that the gating pore current may have an impact on cell morphology (Wu et al., 2011, 2012).

Previous work on Shaker-type and Na$_v$ channels revealed that gating pore current pathways open in a state-dependent manner, i.e., in the specific state in which the mutated arginine is in the GCTC and in which the disruption of the salt bridge leads to a junction of the two water crevices (Tombola et al., 2005, 2006, 2007; Sokolov et al., 2007; Delemotte et al., 2010; Gamal El-Din et al., 2010; Gosselin-Badaroudine et al., 2012a; Khalili-Araghi et al., 2012; Moreau et al., 2014b). Two different states fulfill these conditions for the R222Q and R225W mutants (β for R225W and γ for R222Q), raising the possibility that the relative population of the various states at a given transmembrane voltage is also altered by the mutations. Indeed, although the VSD is expected to be in its fully activated state (at 40 mV), gating pore currents are observed for R222Q and R225W mutant channels, indicating that the mutated residue is still located in the GCTC. This suggests that the "fully activated" state for these mutant channels might be different from the "fully activated" state of WT channels.

Similar depolarization-activated gating pores have been shown to be permeant at hyperpolarized potentials after long depolarization periods (Sokolov et al., 2008; Fan et al., 2013; Gamal El-Din et al., 2014; Groome et al., 2014). This phenomenon would be caused by S4 segment immobilization whereas, in WT condition, after depolarization, the S4 segments are expected to rapidly reach their resting conformation (Cha et al., 1999). Our results indeed show that after the depolarization period mimicking the cardiac AP duration, the mutated S4 segments remain trapped in their conductive conformations at hyperpolarized voltages (Fig. 6).
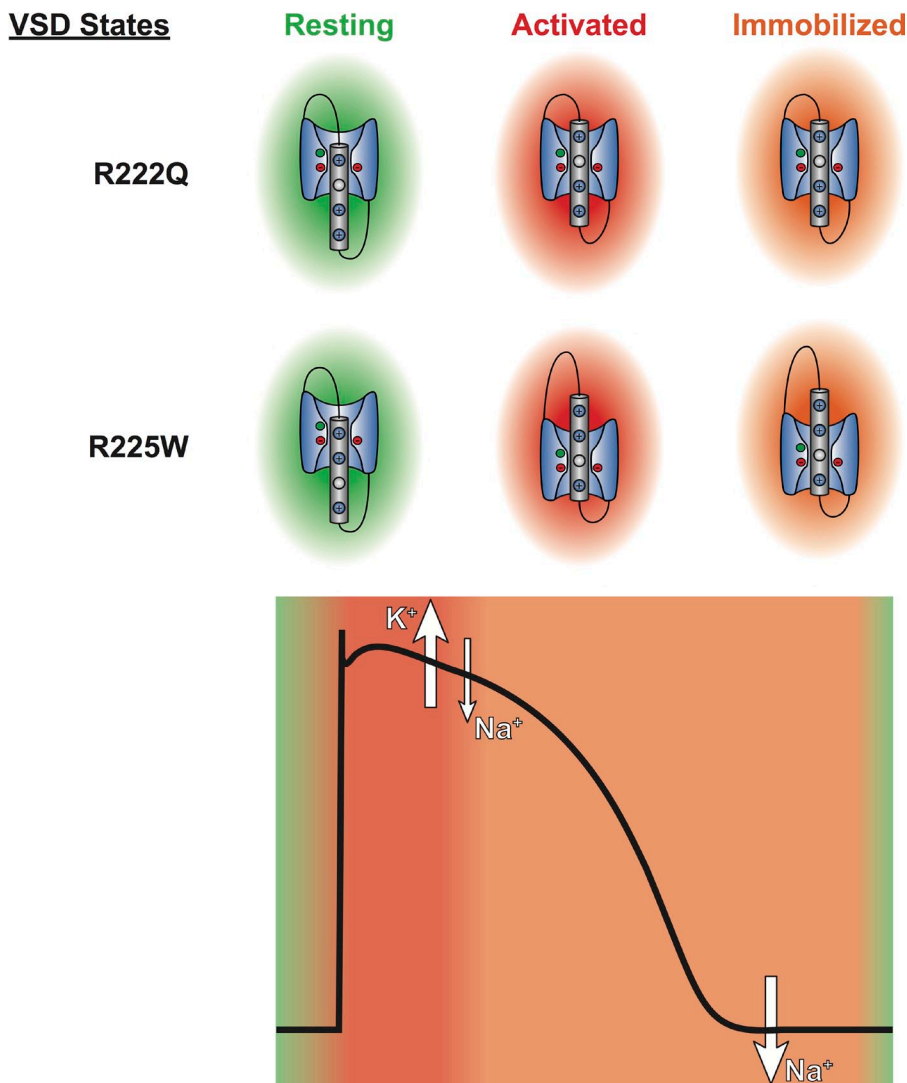

Figure 8. The gating pore current generated by R222Q and R225W mutations is permeant in both activated and resting states. The VSD of domain I of mutated Na$_v$1.5 is shown in their resting (green), activated (red), and immobilized (orange) states. These states are represented during the cardiac AP. The gating pore permeation pathway is open during the plateau phase of the AP, leading to an outward K$^+$ leak and an inward Na$^+$ leak. Because of S4 immobilization, the gating pore is also permeant to Na$^+$ at the end of the AP.

Based on physiological ionic homeostasis, the R222Q and R225W gating pores would cause an outward K^+ current and an inward Na^+ current during the cardiac AP (Fig. 8). Because of S4 segment immobilization, at the end of the cardiac AP, the gating pore would be temporarily permeable to Na^+ ions (Fig. 8). In this case, the Na^+ leak would cause a Na^+ overload, as observed in HypoPP patients (Jurkat-Rott et al., 2009; Fan et al., 2013). The potential effects of this Na^+ overload are schematized in Fig. S3. The Na^+ leak may counterbalance K_{ir} channels, limiting repolarizing currents (Tricarico and Camerino, 2011; Moreau et al., 2014a). This Na^+ leak may also activate reverse Na^+/Ca^{2+} exchange (Remme and Wilde, 2014), leading to a Ca^{2+} overload. A Ca^{2+} overload would modulate Ca^{2+} affinity of troponins, which would disturb the contractile apparatus (Liu et al., 2012). Ca^{2+} overload would also disrupt intercellular communication (by blocking connexins) (Bukauskas et al., 2001), and disrupt Ca^{2+} homeostasis through the ryanodine and IP_3 receptors. However, the exact downstream consequences of such gating pores remain to be elucidated. The study of animal models could highlight the exact pathophysiological consequences of cation leaks through gating pores.

In conclusion, our results demonstrate that R2 and R3 mutations in S4 DI of $Na_v1.5$ channels lead to the creation of a gating pore. Such gating pores have already been observed with the $Na_v1.5$ R219H mutation and other $Na_v1.4$ and $Ca_v1.1$ mutations associated with Hypo or NormoPP (Gosselin-Badaroudine et al., 2012a; Moreau et al., 2014a). Collectively, our data suggest that gating pores caused by mutations in $Na_v1.5$ VSD could constitute a novel pathological mechanism at the origin of an atypical clinical phenotype combining complex cardiac arrhythmias and dilatation.

REFERENCES

Amaral, C., V. Carnevale, M.L. Klein, and W. Treptow. 2012. Exploring conformational states of the bacterial voltage-gated sodium channel NavAb via molecular dynamics simulations. *Proc. Natl. Acad. Sci. USA.* 109:21336–21341. http://dx.doi.org/10.1073/pnas.1218087109

Amin, A.S., A. Asghari-Roodsari, and H.L. Tan. 2010. Cardiac sodium channelopathies. *Pflugers Arch.* 460:223–237. http://dx.doi.org/10.1007/s00424-009-0761-0

Berger, T.K., and E.Y. Isacoff. 2011. The pore of the voltage-gated proton channel. *Neuron.* 72:991–1000. http://dx.doi.org/10.1016/j.neuron.2011.11.014

Bezzina, C.R., and C.A. Remme. 2008. Dilated cardiomyopathy due to sodium channel dysfunction: What is the connection? *Circ Arrhythm Electrophysiol.* 1:80–82. http://dx.doi.org/10.1161/CIRCEP.108.791434

Bezzina, C.R., M.B. Rook, W.A. Groenewegen, L.J. Herfst, A.C. van der Wal, J. Lam, H.J. Jongsma, A.A. Wilde, and M.M. Mannens. 2003. Compound heterozygosity for mutations (W156X and R225W) in SCN5A associated with severe cardiac conduction disturbances and degenerative changes in the conduction system. *Circ. Res.* 92:159–168. http://dx.doi.org/10.1161/01.RES.0000052672.97759.36

Blanchet, J., and M. Chahine. 2007. Accessibility of four arginine residues on the S4 segment of the *Bacillus halodurans* sodium channel. *J. Membr. Biol.* 215:169–180. http://dx.doi.org/10.1007/s00232-007-9016-1

Bukauskas, F.F., A. Bukauskiene, M.V. Bennett, and V.K. Verselis. 2001. Gating properties of gap junction channels assembled from connexin43 and connexin43 fused with green fluorescent protein. *Biophys. J.* 81:137–152. http://dx.doi.org/10.1016/S0006-3495(01)75687-1

Cha, A., P.C. Ruben, A.L. George Jr., E. Fujimoto, and F. Bezanilla. 1999. Voltage sensors in domains III and IV, but not I and II, are immobilized by Na^+ channel fast inactivation. *Neuron.* 22:73–87. http://dx.doi.org/10.1016/S0896-6273(00)80680-7

Chahine, M., S. Pilote, V. Pouliot, H. Takami, and C. Sato. 2004. Role of arginine residues on the S4 segment of the *Bacillus halodurans* Na^+ channel in voltage-sensing. *J. Membr. Biol.* 201:9–24. http://dx.doi.org/10.1007/s00232-004-0701-z

Cheng, J., A. Morales, J.D. Siegfried, D. Li, N. Norton, J. Song, J. Gonzalez-Quintana, J.C. Makielski, and R.E. Hershberger. 2010. SCN5A rare variants in familial dilated cardiomyopathy decrease peak sodium current depending on the common polymorphism H558R and common splice variant Q1077del. *Clin. Transl. Sci.* 3:287–294. http://dx.doi.org/10.1111/j.1752-8062.2010.00249.x

Darden, T., D. York, and L. Pedersen. 1993. Particle Mesh Ewald: An $N\cdot\log(N)$ method for Ewald sums in large systems. *J. Chem. Phys.* 98:10089–10092. http://dx.doi.org/10.1063/1.464397

Delemotte, L., W. Treptow, M.L. Klein, and M. Tarek. 2010. Effect of sensor domain mutations on the properties of voltage-gated ion channels: Molecular dynamics studies of the potassium channel Kv1.2. *Biophys. J.* 99:L72–L74. http://dx.doi.org/10.1016/j.bpj.2010.08.069

Delemotte, L., M. Tarek, M.L. Klein, C. Amaral, and W. Treptow. 2011. Intermediate states of the Kv1.2 voltage sensor from atomistic molecular dynamics simulations. *Proc. Natl. Acad. Sci. USA.* 108:6109–6114. http://dx.doi.org/10.1073/pnas.1102724108

Deschênes, I., G. Baroudi, M. Berthet, I. Barde, T. Chalvidan, I. Denjoy, P. Guicheney, and M. Chahine. 2000. Electrophysiological characterization of SCN5A mutations causing long QT (E1784K) and Brugada (R1512W and R1432G) syndromes. *Cardiovasc. Res.* 46:55–65. http://dx.doi.org/10.1016/S0008-6363(00)00006-7

Eswar, N., B. Webb, M.A. Marti-Renom, M.S. Madhusudhan, D. Eramian, M.Y. Shen, U. Pieper, and A. Sali. 2006. Comparative protein structure modeling using Modeller. *Curr. Protoc. Bioinformatics.* 5:5.6.

Fan, C., F. Lehmann-Horn, M.A. Weber, M. Bednarz, J.R. Groome, M.K. Jonsson, and K. Jurkat-Rott. 2013. Transient compartment-like syndrome and normokalaemic periodic paralysis due to a Ca(v)1.1 mutation. *Brain.* 136:3775–3786. http://dx.doi.org/10.1093/brain/awt300

Feller, S.E., and A.D. MacKerell Jr. 2000. An improved empirical potential energy function for molecular simulations of

phospholipids. *J. Phys. Chem. B.* 104:7510–7515. http://dx.doi.org/10.1021/jp0007843

Gamal El-Din, T.M., H. Heldstab, C. Lehmann, and N.G. Greeff. 2010. Double gaps along Shaker S4 demonstrate omega currents at three different closed states. *Channels (Austin).* 4:93–100. http://dx.doi.org/10.4161/chan.4.2.10672

Gamal El-Din, T.M., G.Q. Martinez, J. Payandeh, T. Scheuer, and W.A. Catterall. 2013. A gating charge interaction required for late slow inactivation of the bacterial sodium channel NavAb. *J. Gen. Physiol.* 142:181–190. http://dx.doi.org/10.1085/jgp.201311012

Gamal El-Din, T.M., T. Scheuer, and W.A. Catterall. 2014. Tracking S4 movement by gating pore currents in the bacterial sodium channel NaChBac. *J. Gen. Physiol.* 144:147–157. http://dx.doi.org/10.1085/jgp.201411210

Gellens, M.E., A.L. George Jr., L.Q. Chen, M. Chahine, R. Horn, R.L. Barchi, and R.G. Kallen. 1992. Primary structure and functional expression of the human cardiac tetrodotoxin-insensitive voltage-dependent sodium channel. *Proc. Natl. Acad. Sci. USA.* 89:554–558. http://dx.doi.org/10.1073/pnas.89.2.554

Gosselin-Badaroudine, P., L. Delemotte, A. Moreau, M.L. Klein, and M. Chahine. 2012a. Gating pore currents and the resting state of Nav1.4 voltage sensor domains. *Proc. Natl. Acad. Sci. USA.* 109:19250–19255. http://dx.doi.org/10.1073/pnas.1217990109

Gosselin-Badaroudine, P., D.I. Keller, H. Huang, V. Pouliot, A. Chatelier, S. Osswald, M. Brink, and M. Chahine. 2012b. A proton leak current through the cardiac sodium channel is linked to mixed arrhythmia and the dilated cardiomyopathy phenotype. *PLoS ONE.* 7:e38331. http://dx.doi.org/10.1371/journal.pone.0038331

Gosselin-Badaroudine, P., A. Moreau, and M. Chahine. 2014. Na$_v$1.5 mutations linked to dilated cardiomyopathy phenotypes: Is the gating pore current the missing link? *Channels (Austin).* 8:90–94. http://dx.doi.org/10.4161/chan.27179

Groome, J.R., F. Lehmann-Horn, C. Fan, M. Wolf, V. Winston, L. Merlini, and K. Jurkat-Rott. 2014. NaV1.4 mutations cause hypokalaemic periodic paralysis by disrupting IIIS4 movement during recovery. *Brain.* 137:998–1008. http://dx.doi.org/10.1093/brain/awu015

Henrion, U., J. Renhorn, S.I. Börjesson, E.M. Nelson, C.S. Schwaiger, P. Bjelkmar, B. Wallner, E. Lindahl, and F. Elinder. 2012. Tracking a complete voltage-sensor cycle with metal-ion bridges. *Proc. Natl. Acad. Sci. USA.* 109:8552–8557. http://dx.doi.org/10.1073/pnas.1116938109

Huang, H., S.G. Priori, C. Napolitano, M.E. O'Leary, and M. Chahine. 2011. Y1767C, a novel SCN5A mutation, induces a persistent Na$^+$ current and potentiates ranolazine inhibition of Nav1.5 channels. *Am. J. Physiol. Heart Circ. Physiol.* 300:H288–H299. http://dx.doi.org/10.1152/ajpheart.00539.2010

Izaguirre, J.A., S. Reich, and R.D. Skeel. 1999. Longer time steps for molecular dynamics. *J. Chem. Phys.* 110:9853–9864. http://dx.doi.org/10.1063/1.478995

Jensen, M.O., V. Jogini, D.W. Borhani, A.E. Leffler, R.O. Dror, and D.E. Shaw. 2012. Mechanism of voltage gating in potassium channels. *Science.* 336:229–233. http://dx.doi.org/10.1126/science.1216533

Jogini, V., and B. Roux. 2007. Dynamics of the Kv1.2 voltage-gated K$^+$ channel in a membrane environment. *Biophys. J.* 93:3070–3082. http://dx.doi.org/10.1529/biophysj.107.112540

Jorgensen, W.L., J. Chandrasekhar, J.D. Madura, R.W. Impey, and M.L. Klein. 1983. Comparison of simple potential functions for simulating liquid water. *J. Chem. Phys.* 79:926–935. http://dx.doi.org/10.1063/1.445869

Jurkat-Rott, K., M.A. Weber, M. Fauler, X.H. Guo, B.D. Holzherr, A. Paczulla, N. Nordsborg, W. Joechle, and F. Lehmann-Horn. 2009. K$^+$-dependent paradoxical membrane depolarization and Na$^+$

overload, major and reversible contributors to weakness by ion channel leaks. *Proc. Natl. Acad. Sci. USA.* 106:4036–4041. http://dx.doi.org/10.1073/pnas.0811277106

Khalili-Araghi, F., E. Tajkhorshid, B. Roux, and K. Schulten. 2012. Molecular dynamics investigation of the ω-current in the Kv1.2 voltage sensor domains. *Biophys. J.* 102:258–267. http://dx.doi.org/10.1016/j.bpj.2011.10.057

Krepkiy, D., M. Mihailescu, J.A. Freites, E.V. Schow, D.L. Worcester, K. Gawrisch, D.J. Tobias, S.H. White, and K.J. Swartz. 2009. Structure and hydration of membranes embedded with voltage-sensing domains. *Nature.* 462:473–479. http://dx.doi.org/10.1038/nature08542

Lacroix, J.J., S.A. Pless, L. Maragliano, F.V. Campos, J.D. Galpin, C.A. Ahern, B. Roux, and F. Bezanilla. 2012. Intermediate state trapping of a voltage sensor. *J. Gen. Physiol.* 140:635–652. http://dx.doi.org/10.1085/jgp.201210827

Lacroix, J.J., H.C. Hyde, F.V. Campos, and F. Bezanilla. 2014. Moving gating charges through the gating pore in a Kv channel voltage sensor. *Proc. Natl. Acad. Sci. USA.* 111:E1950–E1959. http://dx.doi.org/10.1073/pnas.1406161111

Larkin, M.A., G. Blackshields, N.P. Brown, R. Chenna, P.A. McGettigan, H. McWilliam, F. Valentin, I.M. Wallace, A. Wilm, R. Lopez, et al. 2007. Clustal W and Clustal X version 2.0. *Bioinformatics.* 23:2947–2948. http://dx.doi.org/10.1093/bioinformatics/btm404

Laurent, G., S. Saal, M.Y. Amarouch, D.M. Béziau, R.F. Marsman, L. Faivre, J. Barc, C. Dina, G. Bertaux, O. Barthez, et al. 2012. Multifocal ectopic Purkinje-related premature contractions: A new SCN5A-related cardiac channelopathy. *J. Am. Coll. Cardiol.* 60:144–156. http://dx.doi.org/10.1016/j.jacc.2012.02.052

Li, Q., S. Wanderling, P. Sompornpisut, and E. Perozo. 2014. Structural basis of lipid-driven conformational transitions in the KvAP voltage-sensing domain. *Nat. Struct. Mol. Biol.* 21:160–166. http://dx.doi.org/10.1038/nsmb.2747

Lin, M.C., J.Y. Hsieh, A.F. Mock, and D.M. Papazian. 2011. R1 in the Shaker S4 occupies the gating charge transfer center in the resting state. *J. Gen. Physiol.* 138:155–163. http://dx.doi.org/10.1085/jgp.201110642

Liu, B., S.B. Tikunova, K.P. Kline, J.K. Siddiqui, and J.P. Davis. 2012. Disease-related cardiac troponins alter thin filament Ca^{2+} association and dissociation rates. *PLoS ONE.* 7:e38259. http://dx.doi.org/10.1371/journal.pone.0038259

MacKerell, A.D., Jr., D. Bashford, M. Bellott, R.L. Dunbrack Jr., J.D. Evanseck, M.J. Field, S. Fischer, J. Gao, H. Guo, S. Ha, et al. 1998. All-atom empirical potential for molecular modeling and dynamics studies of proteins. *J. Phys. Chem. B.* 102:3586–3616. http://dx.doi.org/10.1021/jp973084f

MacKerell, A.D., Jr., M. Feig, and C.L. Brooks III. 2004. Extending the treatment of backbone energetics in protein force fields: Limitations of gas-phase quantum mechanics in reproducing protein conformational distributions in molecular dynamics simulations. *J. Comput. Chem.* 25:1400–1415. http://dx.doi.org/10.1002/jcc.20065

Mann, S.A., M.L. Castro, M. Ohanian, G. Guo, P. Zodgekar, A. Sheu, K. Stockhammer, T. Thompson, D. Playford, R. Subbiah, et al. 2012. R222Q SCN5A mutation is associated with reversible ventricular ectopy and dilated cardiomyopathy. *J. Am. Coll. Cardiol.* 60:1566–1573. http://dx.doi.org/10.1016/j.jacc.2012.05.050

Matthews, E., R. Labrum, M.G. Sweeney, R. Sud, A. Haworth, P.F. Chinnery, G. Meola, S. Schorge, D.M. Kullmann, M.B. Davis, and M.G. Hanna. 2009. Voltage sensor charge loss accounts for most cases of hypokalemic periodic paralysis. *Neurology.* 72:1544–1547. http://dx.doi.org/10.1212/01.wnl.0000342387.65477.46

McNair, W.P., G. Sinagra, M.R. Taylor, A. Di Lenarda, D.A. Ferguson, E.E. Salcedo, D. Slavov, X. Zhu, J.H. Caldwell, and L. Mestroni, and Familial Cardiomyopathy Registry Research Group. 2011. SCN5A mutations associate with arrhythmic dilated cardiomyopathy

and commonly localize to the voltage-sensing mechanism. *J. Am. Coll. Cardiol.* 57:2160–2168. http://dx.doi.org/10.1016/j.jacc.2010.09.084

Miceli, F., M.V. Soldovieri, C.C. Hernandez, M.S. Shapiro, L. Annunziato, and M. Taglialatela. 2008. Gating consequences of charge neutralization of arginine residues in the S4 segment of K(v)7.2, an epilepsy-linked K⁺ channel subunit. *Biophys. J.* 95:2254–2264. http://dx.doi.org/10.1529/biophysj.107.128371

Miceli, F., E. Vargas, F. Bezanilla, and M. Taglialatela. 2012. Gating currents from Kv7 channels carrying neuronal hyperexcitability mutations in the voltage-sensing domain. *Biophys. J.* 102:1372–1382. http://dx.doi.org/10.1016/j.bpj.2012.02.004

Moreau, A., P. Gosselin-Badaroudine, and M. Chahine. 2014a. Biophysics, pathophysiology, and pharmacology of ion channel gating pores. *Front Pharmacol.* 5:53. http://dx.doi.org/10.3389/fphar.2014.00053

Moreau, A., P. Gosselin-Badaroudine, and M. Chahine. 2014b. Molecular biology and biophysical properties of ion channel gating pores. *Q. Rev. Biophys.* 47:364–388. http://dx.doi.org/10.1017/S0033583514000109

Nair, K., R. Pekhletski, L. Harris, M. Care, C. Morel, T. Farid, P.H. Backx, E. Szabo, and K. Nanthakumar. 2012. Escape capture bigeminy: Phenotypic marker of cardiac sodium channel voltage sensor mutation R222Q. *Heart Rhythm.* 9:1681–1688. http://dx.doi.org/10.1016/j.hrthm.2012.06.029

Park, Y.H., and J.B. Kim. 2010. An atypical phenotype of hypokalemic periodic paralysis caused by a mutation in the sodium channel gene SCN4A. *Korean J Pediatr.* 53:909–912. http://dx.doi.org/10.3345/kjp.2010.53.10.909

Payandeh, J., T. Scheuer, N. Zheng, and W.A. Catterall. 2011. The crystal structure of a voltage-gated sodium channel. *Nature.* 475:353–358. http://dx.doi.org/10.1038/nature10238

Phillips, J.C., R. Braun, W. Wang, J. Gumbart, E. Tajkhorshid, E. Villa, C. Chipot, R.D. Skeel, L. Kalé, and K. Schulten. 2005. Scalable molecular dynamics with NAMD. *J. Comput. Chem.* 26:1781–1802. http://dx.doi.org/10.1002/jcc.20289

Ramsey, I.S., Y. Mokrab, I. Carvacho, Z.A. Sands, M.S. Sansom, and D.E. Clapham. 2010. An aqueous H⁺ permeation pathway in the voltage-gated proton channel Hv1. *Nat. Struct. Mol. Biol.* 17:869–875. http://dx.doi.org/10.1038/nsmb.1826

Remme, C.A., and A.A. Wilde. 2014. Targeting sodium channels in cardiac arrhythmia. *Curr. Opin. Pharmacol.* 15:53–60. http://dx.doi.org/10.1016/j.coph.2013.11.014

Ruan, Y., N. Liu, and S.G. Priori. 2009. Sodium channel mutations and arrhythmias. *Nat. Rev. Cardiol.* 6:337–348. http://dx.doi.org/10.1038/nrcardio.2009.44

Schwaiger, C.S., S.I. Börjesson, B. Hess, B. Wallner, F. Elinder, and E. Lindahl. 2012. The free energy barrier for arginine gating charge translation is altered by mutations in the voltage sensor domain. *PLoS ONE.* 7:e45880. http://dx.doi.org/10.1371/journal.pone.0045880

Sokolov, S., T. Scheuer, and W.A. Catterall. 2007. Gating pore current in an inherited ion channelopathy. *Nature.* 446:76–78. http://dx.doi.org/10.1038/nature05598

Sokolov, S., T. Scheuer, and W.A. Catterall. 2008. Depolarization-activated gating pore current conducted by mutant sodium channels in potassium-sensitive normokalemic periodic paralysis. *Proc. Natl. Acad. Sci. USA.* 105:19980–19985. http://dx.doi.org/10.1073/pnas.0810562105

Struyk, A.F., and S.C. Cannon. 2007. A Na⁺ channel mutation linked to hypokalemic periodic paralysis exposes a proton-selective gating pore. *J. Gen. Physiol.* 130:11–20. http://dx.doi.org/10.1085/jgp.200709755

Tao, X., A. Lee, W. Limapichat, D.A. Dougherty, and R. MacKinnon. 2010. A gating charge transfer center in voltage sensors. *Science.* 328:67–73. http://dx.doi.org/10.1126/science.1185954

Tombola, F., M.M. Pathak, and E.Y. Isacoff. 2005. Voltage-sensing arginines in a potassium channel permeate and occlude cation-selective pores. *Neuron.* 45:379–388. http://dx.doi.org/10.1016/j.neuron.2004.12.047

Tombola, F., M.M. Pathak, and E.Y. Isacoff. 2006. How does voltage open an ion channel? *Annu. Rev. Cell Dev. Biol.* 22:23–52. http://dx.doi.org/10.1146/annurev.cellbio.21.020404.145837

Tombola, F., M.M. Pathak, P. Gorostiza, and E.Y. Isacoff. 2007. The twisted ion-permeation pathway of a resting voltage-sensing domain. *Nature.* 445:546–549. http://dx.doi.org/10.1038/nature05396

Treptow, W., and M. Tarek. 2006. Environment of the gating charges in the Kv1.2 Shaker potassium channel. *Biophys. J.* 90:L64–L66. http://dx.doi.org/10.1529/biophysj.106.080754

Tricarico, D., and D.C. Camerino. 2011. Recent advances in the pathogenesis and drug action in periodic paralyses and related channelopathies. *Front Pharmacol.* 2:8. http://dx.doi.org/10.3389/fphar.2011.00008

Vargas, E., V. Yarov-Yarovoy, F. Khalili-Araghi, W.A. Catterall, M.L. Klein, M. Tarek, E. Lindahl, K. Schulten, E. Perozo, F. Bezanilla, and B. Roux. 2012. An emerging consensus on voltage-dependent gating from computational modeling and molecular dynamics simulations. *J. Gen. Physiol.* 140:587–594. http://dx.doi.org/10.1085/jgp.201210873

Wood, M.L., E.V. Schow, J.A. Freites, S.H. White, F. Tombola, and D.J. Tobias. 2012. Water wires in atomistic models of the Hv1 proton channel. *Biochim. Biophys. Acta.* 1818:286–293. http://dx.doi.org/10.1016/j.bbamem.2011.07.045

Wu, F., W. Mi, D.K. Burns, Y. Fu, H.F. Gray, A.F. Struyk, and S.C. Cannon. 2011. A sodium channel knockin mutant (NaV1.4-R669H) mouse model of hypokalemic periodic paralysis. *J. Clin. Invest.* 121:4082–4094. http://dx.doi.org/10.1172/JCI57398

Wu, F., W. Mi, E.O. Hernández-Ochoa, D.K. Burns, Y. Fu, H.F. Gray, A.F. Struyk, M.F. Schneider, and S.C. Cannon. 2012. A calcium channel mutant mouse model of hypokalemic periodic paralysis. *J. Clin. Invest.* 122:4580–4591. http://dx.doi.org/10.1172/JCI66091

Yarov-Yarovoy, V., P.G. DeCaen, R.E. Westenbroek, C.Y. Pan, T. Scheuer, D. Baker, and W.A. Catterall. 2012. Structural basis for gating charge movement in the voltage sensor of a sodium channel. *Proc. Natl. Acad. Sci. USA.* 109:E93–E102. http://dx.doi.org/10.1073/pnas.1118434109